Volume 12
Number 6
21 March 2024
Pages 1337-1606

Biomaterials Science

rsc.li/biomaterials-science

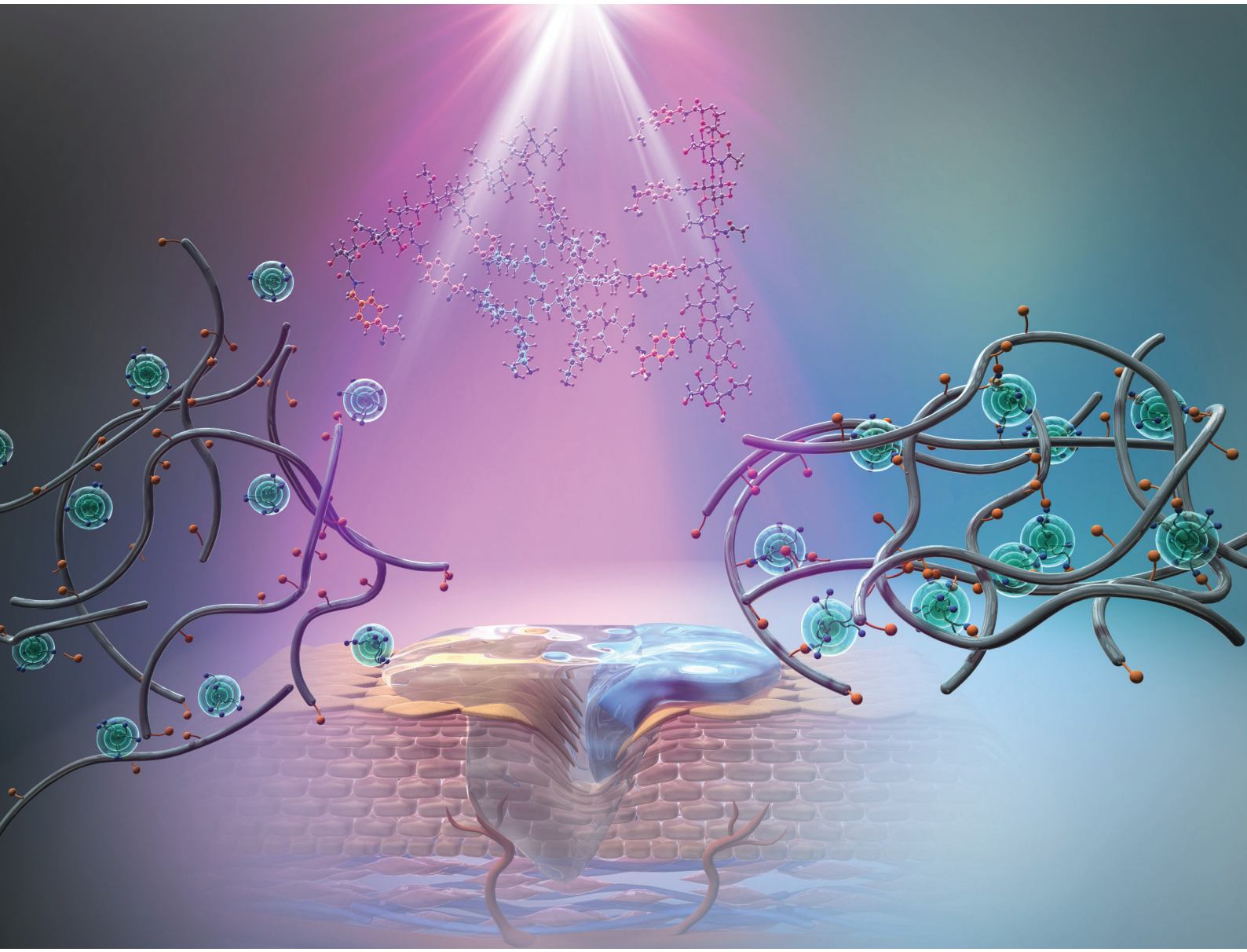

ISSN 2047-4849

ROYAL SOCIETY OF CHEMISTRY

PAPER

Taichi Ito *et al.*

Injectable, shear-thinning, photocrosslinkable, and tissue-adhesive hydrogels composed of diazirine-modified hyaluronan and dendritic polyethyleneimine

European Society for Biomaterials

Biomaterials Science

ROYAL SOCIETY OF CHEMISTRY

PAPER

View Article Online
View Journal | View Issue

Cite this: *Biomater. Sci.*, 2024, **12**, 1454

Injectable, shear-thinning, photocrosslinkable, and tissue-adhesive hydrogels composed of diazirine-modified hyaluronan and dendritic polyethyleneimine†

Arvind K. Singh Chandel,[a] Athira Sreedevi Madhavikutty,[a] Saki Okada,[a] Zhang Qiming,[a] Natsuko F. Inagaki,[a] Seiichi Ohta[a,b] and Taichi Ito *[a,b,c]

In the present study, we report the first synthesis of diazirine-modified hyaluronic acid (HA–DAZ). In addition, we also produced a precursor polymer solution composed of HA–DAZ and dendritic polyethyleneimine (DPI) that showed strong shear-thinning properties. Furthermore, its viscosity was strongly reduced (*i.e.*, from 5×10^5 mPa s at 10^{-3} s^{-1} to 6×10^1 mPa s at 10^3 s^{-1}), substantially, which enhanced solution injectability using a 21 G needle. After ultraviolet irradiation at 365 nm and 6 mW cm^{-2}, the HA–DAZ/DPI solution achieved rapid gelation, as measured using the stirring method, and its gelation time decreased from 200 s to 9 s as the total concentrations of HA–DAZ and DPI increased. Following UV irradiation, the storage modulus increased from 40 to 200 Pa. In addition, reversible sol–gel transition and self-healing properties were observed even after UV irradiation. This suggests that the HA–DAZ/DPI hydrogel was crosslinked in multiple ways, *i.e.*, *via* covalent bonding between the diazirine and amine groups and *via* intermolecular interactions, including hydrogen bonding, electrostatic interactions, and hydrophobic interactions. A lap shear test showed that the HA–DAZ/DPI hydrogel exhibited strong adhesiveness as a fibrin glue following UV irradiation. Finally, the HA–DAZ/DPI hydrogel showed higher tissue reinforcement than fibrin glue in an *ex vivo* burst pressure test of the porcine esophageal mucosa.

Received 3rd August 2023,
Accepted 21st December 2023

DOI: 10.1039/d3bm01279d

rsc.li/biomaterials-science

1. Introduction

Hyaluronic acid (HA), also known as hyaluronan, is a major component of the extracellular matrix in vertebrate tissues.[1,2] Due to its highly hydrated structure and unique viscoelastic properties in the water, HA has been well-studied in various medical applications, *e.g.*, eye drops, osteoarthritis treatments, and antiperitoneal adhesion. HA is composed of D-glucuronic acid and *N*-acetyl-D-glucosamine. The carboxy group of D-glucuronic acid is important for the chemical modifications required to synthesize HA derivatives.[3] Using these HA hydrogels, several *in situ* cross-linkable hydrogels[4] have been produced *via* Schiff base formation,[5] disulfide bonding,[6] Michael addition,[7] copper-free click reactions[8] and enzymatic crosslinking using HRP and H_2O_2.[9] Many potential medical use cases of hydrogels with these properties have been proposed.

Injectable and photocrosslinkable hydrogels have numerous medical uses, including anti-esophagus stenosis or hemostasis after endoscopic submucosal dissection,[10] wound headlining,[11,12] dermatological fillers,[13] viscosity-supplementation for osteoarthritis treatment,[14] ophthalmic drug delivery formulations,[15] 3D printing,[16] and tissue engineering scaffolds.[17] A single-component precursor polymer solution is injected *via* a catheter or syringe, and then irradiated to achieve crosslinking. Due to the high biocompatibility of HA, several injectable and photocrosslinkable HA-based hydrogels[18] have been produced. One popular approach involves using HA modified with glycidyl methacrylate[19] or *N*-(3-aminopropyl)methacrylamide[20] to achieve light-induced radical polymerization. In addition, photodimerization of HA–cinnamate,[21] the pectin-conjugated norbornene photo-click reaction,[22] imine ligation *via* *o*-nitrobenzyl,[23] the S-nitrosylation coupling reaction,[24] the [2 + 2] photocycloaddition reaction of coumarin,[25] the thiol–ene photo-click reaction,[26] the Diels–Alder reaction, and furan under the catalysis of lithium phenyl-2,4,6-trimethylbenzoylphosphinate-[27] have all been used for

[a]*Department of Chemical System Engineering, School of Engineering, The University of Tokyo, 7-3-1 Hongo, Bunkyo-ku, Tokyo 113-8656, Japan.*
E-mail: itotaichi@g.ecc.u-tokyo.ac.jp
[b]*Department of Bioengineering, School of Engineering, The University of Tokyo, 7-3-1 Hongo, Bunkyo-ku, Tokyo 113-8656, Japan*
[c]*Radiology and Biomedical Engineering, School of Medicine, The University of Tokyo, 7-3-1 Hongo, Bunkyo-ku, Tokyo 113-8656, Japan*

† Electronic supplementary information (ESI) available. See DOI: https://doi.org/10.1039/d3bm01279d

photocrosslinkable systems. However, most of these photocrosslinking systems use photoinitiators[18–20,22,23,25,26] that may induce potential cytotoxicity. They also require irradiation using 250–370 nm UV light, which can damage cells.[21,22,24]

Diazirine[28]-based photocrosslinked hydrogels are of interest because diazirines react under biologically safe long UV wavelengths (*i.e.*, 350–360 nm) which causes minimal photodamage to cells. In addition, diazirine-based photocrosslinking does not require the addition of photoinitiators and produces only nitrogen as a byproduct; these advantages minimize the potential toxicity of hydrogel formation. Moreover, diazirines are stable in both acids and bases, do not react with common nucleophiles and electrophiles, and can be stored at room temperature.[29] These characteristics therefore also make diazirine an important tool for photoaffinity labeling. Although the properties of diazirine make it a suitable component for photocrosslinkable hydrogels, few studies have reported the use of diazirine in photoreactive hydrogels. For example, Mogal *et al.*[24] and Gao *et al.*,[30] reported the use of a PAMAM-*g*-diazirine-based photocrosslinkable bioadhesive. In these studies, the authors found that the diazirine moiety reacts quickly with a primary amine under UV-A light (*i.e.*, 365 nm). This means that a diazirine-conjugated polymer and the amine moiety of a tissue protein will crosslink when exposed to biologically safe UV-A light. Moreover, this crosslinking reaction provides adhesion between the polymer and tissue even under wet conditions. Furthermore, the strength of the conjugated diazirine-based adhesive can be tuned by varying the degree of substitution. In addition, Wang *et al.*[31,32] also reported protein–diazirine-based photocrosslinked hydrogels. Therefore a polymer using a diazirine 4-[3-(trifluoromethyl)-3*H*-diazirin-3-yl]benzene hydrophobic moiety combined with a highly hydrophilic HA backbone is ideal for fabricating diazirine-based hydrogels.

In recent years, shear-thinning and self-healing properties[33] have attracted the attention of researchers of injectable gels. The ability to reduce viscosity in high shear rate regions reduces pressure drops and markedly improves injectability. Both features have proven to be useful for the administration of gels through long and thin catheters[34] or in bio-ink applications. Indeed, several HA-based shear-thinning injectable hydrogels[35,36] have been produced as well as bio-inks for use in 3D applications.[37] However, to date no shear-thinning gels produced using diazirine have been reported.

In the present study, we synthesized diazirine-modified HA (HA–DAZ) for the first time. This was then mixed with water-soluble dendritic polyethene imine (DPI) for further photocrosslinking *via* UV-A irradiation at 365 nm (Fig. 1). This compound contains numerous qualities thought to be advantageous for tissue adhesion applications, including the high biocompatibility of the HA backbone, its durability in the absence of an initiator, the relatively long wavelength of the UV light used, and the generation of safe byproducts following DAZ conjugation.

The flow curve of the HA–DAZ/DPI solution was measured using a rheometer to evaluate its injectability and shear-thinning properties, which are important for its ejection through a narrow tube or catheter. Furthermore, the gelation rate and rheological properties of HA–DAZ/DPI hydrogels were measured following photocrosslinking *via* UV-A treatment at 365 nm. The cytocompatibility of HA–DAZ/DPI hydrogels was also assessed using NIH3T3 cells. Finally, the tissue adhesiveness of HA–DAZ/DPI hydrogels was evaluated using a lap shear adhesion test and a burst pressure test.

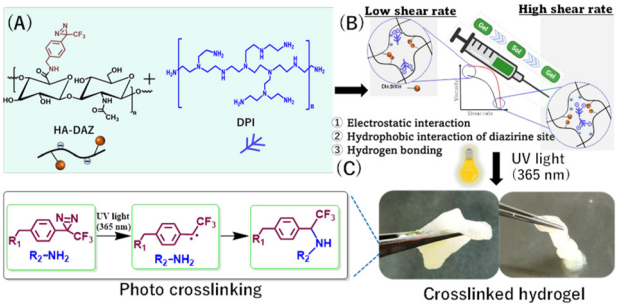

Fig. 1 Diagrams illustrating the present research. (A) An aqueous mixture of diazirine-modified hyaluronic acid (HA–DAZ) and dendritic poly(ethyleneimine) (DPI). (B) Shear-thinning properties of the mixture. (C) Photocrosslinking in the presence of UV light postinjection.

2. Materials and methods

2.1 Materials

HA (molecular weight: 850 kDa) was kindly donated by Denka Co., Ltd (Tokyo, Japan). DPI (Polymin® PS; molecular weight: 750 kDa) was kindly donated by BASF (Ludwigshafen, Germany). Sodium hexametaphosphate, Minimum Essential Medium with Eagle's salts, 4-[3-(trifluoromethyl)-3*H*-diazirin-3-yl]benzylamine hydrochloride (DAZ), and 1-hydroxybenzotriazole hydrate (HOBt) were purchased from Sigma-Aldrich (St Louis, USA). Dulbecco's modified Eagle's medium (DMEM), penicillin–streptomycin–amphotericin B suspension, and fetal bovine serum (FBS) were all purchased from Wako Pure Chemical Ind. (Osaka, Japan). 1-Ethyl-3-(3-(dimethylamino)propyl)carbodiimide hydrochloride (EDC) was purchased from Peptide Institute, Inc. (Osaka, Japan). A dialysis membrane (Spectra/Por; molecular weight cut-off: 6–8 kDa) was purchased from Spectrum Laboratories Inc. (Rancho Dominguez, USA). Normal saline was purchased from Otsuka Pharmaceutical (Tokyo, Japan). Finally, Beriplast® P fibrin glue was purchased from CSL Behring (King of Prussia, USA).

2.2 Synthesis of HA–DAZ

HA–DAZ was prepared using a carbodiimide reaction. Specifically, 0.5 g (0.0013 mol) of HA was dissolved in 150 mL of distilled water. Thereafter, 1.13 g (0.0059 mol) of EDC was dissolved in 10 mL of distilled water and added to the HA solution dropwise. Next, 0.80 g (0.0059 mol) of HOBt was dissolved in 5 mL of DMSO, added to the abovementioned solution, and stirred for 15–20 min. 0.33 g of DAZ was then dissolved in

10 mL of DMSO in the dark and added to the HA solution dropwise. The reaction pH was maintained at 5.5, and the solution was stirred for 20–24 h at room temperature in the dark. The reaction mixture was then subjected to dialysis against pure water for 72 h, during which time dialysis water was periodically replaced with pure water. After dialysis, the dialyzed solution was then lyophilized and a dried sample was stored in an airtight container in the dark at 4 °C.

2.3 Preparation of HA–DAZ and a HA–DAZ/DPI hydrogel

HA–DAZ (1%, w/v) and DPI (3.3%, w/v) solutions were first prepared using distilled water. An equal volume of each solution was mixed in a Petri dish (25 mm) at 25 °C, generating a molar ratio of DAZ (in HA–DAZ) : NH_2 (in DPI) of 1 : 16. The resulting solution was then exposed to 6 mW cm^{-2} UV light generated by a Supercure-204S UV light source (SAN-El Electronic, Osaka, Japan) for five min to obtain a crosslinked hydrogel. We then measured the effect of the prepolymer solution concentration on gelation time. To measure gelation time, we first added 100 μL of an aqueous solution containing HA–DAZ (10 mg mL^{-1}) and DPI (40 mg mL^{-1}) (volume ratio 1 : 1) to a Petri dish and stirred the solution at 300 rpm using a stirrer (RS-1DR; AS ONE, Osaka, Japan) and stir bar (2 × 5 mm). The solution was then exposed to 6 mW cm^{-2} UV light at a wavelength of 365 nm, and the rotation of a magnetic bar was observed *via* a digital camera held at a fixed position during sample mixing. We determined the gelation time as the time taken for the mixture to become a globule.

2.4 Characterization of HA–DAZ and the HA–DAZ/DPI hydrogel

Synthesis of HA–DAZ was confirmed using ^{1}H NMR (JEOL JNM-A500, JEOL, Tokyo, Japan). The ^{1}H NMR was performed using 32 scans with a relaxation time of 8 seconds. Polymers were dissolved in D_2O prior to ^{1}H NMR analysis. The degree of modification of HA–DAZ was then determined by comparing the peak area integration of DAZ and the HA backbone. Subsequently, we obtained Fourier-transform infrared spectroscopy (FT-IR) spectra of HA, HA–DAZ, and DPI using the potassium bromide disk method and an FT-IR-4200ST spectrometer (JASCO, Tokyo, Japan) with a potassium bromide pallet for each polymer. Furthermore, the molecular weight distributions of different polymers were determined *via* gel permeation chromatography (GPC) using a chromatograph equipped with an LC-10ADVP pump (Shimadzu, Tokyo, Japan) and an 830-RI differential refractive index detector (JASCO, Tokyo, Japan) as described previously.[38] All GPC measurements were performed at room temperature using a TSK-Gel GMPWXL column (TOSOH, Tokyo, Japan) at a flow rate of 0.5 mL min^{-1}, with a sodium phosphate buffer (0.05 M; adjusted to pH 6.7). NaCl (0.2 M) was used as the eluent. Finally, molecular weights were determined relative to dextran standards (Extrasynthese, Genay, France). Next, the internal morphology of the swelled HA–DAZ/DPI hydrogel was observed using a scanning electron microscope (SEM; S-900, Hitachi, Tokyo, Japan). We calculated the average pore size of the photo-crosslinked HA–DAZ/DPI hydrogel using SEM images. The dynamic light scattering (DLS) technique was used to investigate the different molecular interactions between HA–DAZ and DPI. Briefly, we prepared separate 0.1% (w/v) HA–DAZ and DPI solutions in distilled water, and the hydrodynamic size distributions of HA–DAZ, DPI, and a mixture (1 : 1) were measured at 25 °C by DLS using a Malvern Instruments Zetasizer Nano ZS90.

2.5 Measurements of the rheological properties of HA–DAZ/DPI solutions and the hydrogel

For rheological measurements, equal amounts of HA or HA–DAZ solution and HA–DAZ/DPI solution were injected using a syringe into silicone molds (diameter: 25 mm; depth: 1.0 mm) to achieve a final concentration of HA or HA–DAZ of 3.0% (w/v). Next, the resulting mixture was irradiated using 6 mW cm^{-2} of UV light to obtain homogeneous hydrogel disks. Dynamic oscillatory frequency and strain sweep experiments were then performed using an MCR301 rheometer (Anton Paar, Graz, Austria) using parallel-plate geometry (PP25; diameter: 25 mm; gap = 1.0 mm) for hydrogel samples and cone-plate geometry (CP50-1-27711; diameter: 50 mm; cone angle: 0.976°) for solution samples. All measurements were performed in triplicate using the same setup; we also included a humidity chamber to avoid undue influence of water evaporation. The representative gap was adjusted by compressing the hydrogel until a normal force of approximately 30 mN was achieved. A strain sweep experiment (at 25 °C or 37 °C and 1 Hz) was then performed to determine the yield stress of the precursor solution and the photocrosslinked hydrogel.

2.6 Assessments of the swelling and degradation of the HA–DAZ/DPI hydrogel

Next, we conducted *in vitro* swelling and degradation tests for the photocrosslinked HA–DAZ/DPI hydrogel in pH 7.4, pH 5.0 buffers, and cell culture medium. The initial weight of each sample was measured before experimentation, and the hydrogels were placed in 25 mL of phosphate-buffered saline (PBS) pH 7.4, acetate buffer pH 5.0, and DMEM cell culture at 37 °C. Samples were weighted during incubation at specific intervals. A total of four replications were performed for each condition. Experiments were conducted until the degradation was almost complete.

2.7 Evaluating the cytotoxicity of HA–DAZ and the HA–DAZ/DPI hydrogel

We then assessed the cytotoxicity of the photocrosslinked HA–DAZ/DPI hydrogel using a water-soluble tetrazolium salt (WST-8) assay (Cell Counting Kit 8, Dojindo, Kumamoto, Japan). Briefly, NIH3T3 cells were seeded onto 24-well plates with DMEM supplemented with 1% PSA and 10% FBS growth medium at a density of 3 × 10^4 cells per well. Cells were then allowed to grow for 24 h. A fresh DMEM cell culture medium containing HA or HA–DAZ was then transferred to each well to achieve final polymer concentrations of 0.1, 0.2, 0.5, and 1.0 wt%. The cytotoxicity of HA–DAZ/DPI hydrogels was also

assessed by incubating 50 to 400 mg of hydrogel samples with cells in 500 μL of culture medium. This was performed without direct contact using cell culture inserts (FALCON® Transwell) (Fig. S1A†) or with direct contact (Fig. S1B†). Next, a WST-8 assay to measure cell viability was performed 48 h after incubation at 37 °C with 5% CO_2. Specifically, we added 50 μL of tetrazolium salt solution (WST-8) to each well and incubated at 37 °C for 2 h. The absorbance at 450 nm was then measured using a plate reader (2030 ARVO V3; PerkinElmer, Waltham, MA, USA). Cell viability was then calculated by normalizing the obtained absorbance for each well to that of control wells that contained no test materials according to the following equation:

$$\text{Cell viability}\,(\%) = \frac{\text{Abs}_{\text{sample}} - \text{Abs}_{\text{blank}}}{\text{Abs}_{\text{control}} - \text{Abs}_{\text{blank}}} \times 100$$

here, $\text{Abs}_{\text{sample}}$, $\text{Abs}_{\text{blank}}$, and $\text{Abs}_{\text{control}}$ represent the absorbance values of the sample well, blank well (*i.e.*, containing only culture medium), and positive control well, respectively. The WST assay was conducted using four replicates for each polymer and the hydrogel.

2.8 Measurement of the adhesive strength of the photocrosslinkable HA–DAZ/DPI hydrogel

Next, we evaluated the adhesive strength of the photocrosslinkable HA–DAZ/DPI hydrogel using porcine esophageal mucosa tissue and tensile test equipment (CR-3000EX-S, Sun Scientific Co., Tokyo, Japan). This test was performed using based on a lap shear method reported previously with slight modification.[39] Briefly, two rectangular pieces of porcine esophageal mucosa were cut into rectangles of approximately 40 × 10 mm (length × width). Next, 0.1 mL of a precursor polymer solution was applied uniformly onto the inner surface of each sample of esophageal mucosa, which was then exposed to 6 mW cm^{-2} of UV light for two minutes. Subsequently, both tissue samples were positioned to overlap at the hydrogel site, and UV light was again applied to the interface from both sides for five minutes. After complete gelation, the lap shear test was performed using a dynamic mechanical analyzer with a speed of 5 mm min^{-1}, and the adhesion energy was measured using a 180° peeling test. Adhesion forces were calculated according to the following equation:

$$\text{Adhesion strength}\,(\text{Pa}) = \frac{\text{Force}\,(\text{N})}{\text{Overlaped area}\,(\text{m}^2)}.$$

Four samples were tested for each group.

2.9 Measurement of the burst pressure of the photocrosslinked HA–DAZ/DPI hydrogel

To determine the efficacy of the hydrogel system as a tissue sealant, we performed a burst test using a custom-designed and fabricated apparatus based on another reported by Hong *et al.* with slight modification.[38] Briefly, porcine esophageal mucosa samples were cut into circles with diameters of 50 mm and fixed to the upper surface of a custom-made burst pressure device to seal a small hole (2 mm in diameter). Subsequently, another small hole (2 mm in diameter) was created in the center of the tissue sample using a biopsy punch.[39] Thereafter, 1 mL of a prepolymer mixture solution was applied to the porcine esophageal mucosa circle to cover the hole and 6 mW cm^{-2} of UV light was applied to the prepolymer solution for 5–10 min to achieve crosslinking. A measurement device was then attached to a PBS-filled syringe pump, and PBS solution was then injected into the device at a flow rate of 1 mL min^{-1}. Finally, burst pressure was recorded using a digital pressure gauge. This experiment was repeated to generate four technical replicates.

3. Results

3.1 Synthesis and characterization of HA–DAZ

Here, we synthesized HA–DAZ using a simple carbodiimide conjugation reaction between the amine group of DAZ and the carboxylic group of HA (Fig. 2A). This conjugation was confirmed *via* ^{1}H NMR spectroscopy, where we observed that HA and HA–DAZ showed a peak at 1.88 ppm, representing the $-CH_3$ group of the acetamido moiety of *N*-acetyl-D-glucosamine. Characteristic diazirine peaks were visible at 7.0–7.5 ppm, corresponding to the aromatic 4H proton. Next, the degree of substitution of HA–DAZ was calculated using the peak area integration ratio of the aromatic 4H proton of DAZ (7.0–7.5 ppm) to three protons of the CH_3 group of the acetamido moiety of *N*-acetyl-D-glucosamine at 1.88 ppm (Fig. 2B); the calculated degree of substitution was 30%. We note that the peak between 3.0–3.5 ppm may be derived from an acyl urea side product formed by the carbodiimide reaction. Even after intensive purification *via* dialysis, this side product was difficult to remove. A control experiment was also conducted using a mixture of HA and DAZ without a carbodiimide reagent, followed by ^{1}H NMR measurement before and after dialysis (Fig. S2†). In this test, the peak from DAZ completely disappeared after dialysis, which suggests that DAZ detected in

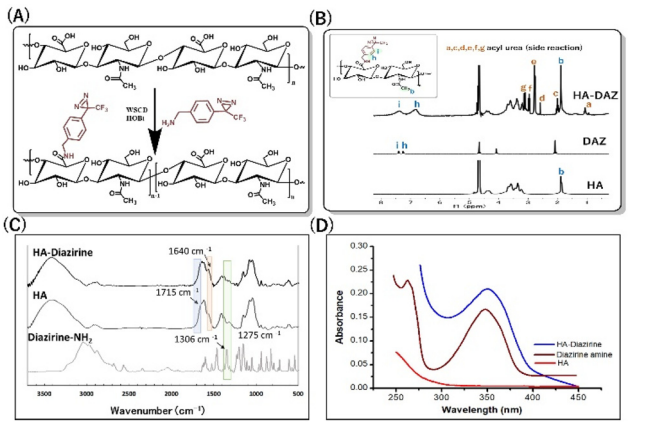

Fig. 2 Synthesis of HA–DAZ. (A) Schematic representation of HA–DAZ synthesis. (B) ^{1}H NMR spectra, (C) FT-IR spectra, and (D) UV-vis spectra of HA, diazirine, and HA–diazirine.

the HA–DAZ sample by ^{1}H NMR was not absorbed but was rather conjugated to the HA backbone.

Next, HA–DAZ was characterized *via* FT-IR spectroscopy. The modification of HA with DAZ was indicated by the emergence of a new peak at 1640 cm^{-1}, which reflected C=O stretching of amide groups. Moreover, the decreased peak intensity of the C=O stretch (1715 cm^{-1}) and the presence of C–N stretching at 1306 cm^{-1} and 1275 cm^{-1} in HA–DAZ indicated that DAZ was conjugated to the carboxylic groups of HA (Fig. 2C). This conjugation was further confirmed by measuring the UV absorbance of the HA and HA–DAZ aqueous solutions. Here, a diazirine peak at 348 nm detected when analyzing the HA–DAZ solution confirmed successful conjugation, and this peak was absent around 348 nm in unmodified HA (Fig. 2D). The degree of substitution was also confirmed by UV spectroscopy using the DAZ calibration curve (Fig. S3†). This calculated degree of substitution was 32.9%, which supported the degree of substitution calculated from the ^{1}H NMR measurement. The molecular weights of HA–DAZ and HA were then compared using GPC. The elution time of HA–DAZ was slightly lower than unmodified HA, which also confirmed the modification of HA with DAZ (Fig. S4†).

3.2 Synthesis and characterization of photocrosslinked HA–DAZ/DPI hydrogels

The photocrosslinked HA–DAZ/DPI hydrogel was obtained by mixing HA–DAZ and DPI solutions and applying UV irradiation at 6 mW cm^{-2} for five minutes (Fig. 3A). Gelation time was measured using the stirring method, and we observed that the magnetic stir bar stopped during the gelation of HA–DAZ (Fig. 3B). The gelation time of the HA–DAZ/DPI hydrogel was then optimized by changing the concentration of the prepolymer solution from 1.0% to 1.5%, 2.0%, 3% and 4% (w/v), but keeping the ratio of HA–DAZ and DPI constant for each phase of the reaction. Here, gelation time depended mainly on the concentration of the prepolymer solution, *i.e.*, it decreased markedly as the concentration of the precursor polymer solution increased.

To prepare the hydrogel and perform further experiments, one ration was selected from all combinations. The same volume of 1 w/v% HA–DAZ and 3.3 w/v% DPI was mixed and thus the final concentration of the polymers was 2.15 w/v%. The molar ratio of DAZ groups to amine groups was 8 to 24. The gelation time and the light irradiation power were 42 ± 4 s and 6 mW cm^{-2}, respectively. Next, we observed that the internal morphology of the lyophilized HA–DAZ/DPI hydrogel as revealed by SEM indicated a highly porous structure, as shown in Fig. 3C. The degree of porosity was also calculated from obtained SEM images, yielding an average pore size of 8.1 μm (Fig. S5†). Gelation was confirmed *via* rheological experiments. A frequency sweep was conducted with an HA–DAZ/DPI precursor polymer solution and a photocrosslinked HA–DAZ/DPI hydrogel using a frequency range from 0.01 to 100 Hz s^{-1}. $G' > G''$ was observed for the crosslinked hydrogel. The precursor polymer solution also showed $G' > G''$, but its G' value was less different than the corresponding G'' value (Fig. 3D).

Interestingly, the HA–DAZ/DPI precursor polymer solution would likely form a weak physical hydrogel due to electrostatic interactions between the negative charge of HA and the positive charge of DPI as well as the hydrophobic interaction of DPI. Despite this, the HA–DAZ/DPI precursor polymer solution could still flow. However, after photocrosslinking the HA–DAZ/DPI precursor polymer solution changed into a stable hydrogel. Moreover, G' increased from 40 to 200 Pa following UV-mediated crosslinking. These values indicate that the materials are soft but may be used as a tissue adhesive. The gelation reaction was also performed using PBS (pH 7.4) buffer and DMEM as a solvent, followed by a rheological measurement *via* frequency sweep test (Fig. S6†). However, similar rheological behavior was observed in both cases.

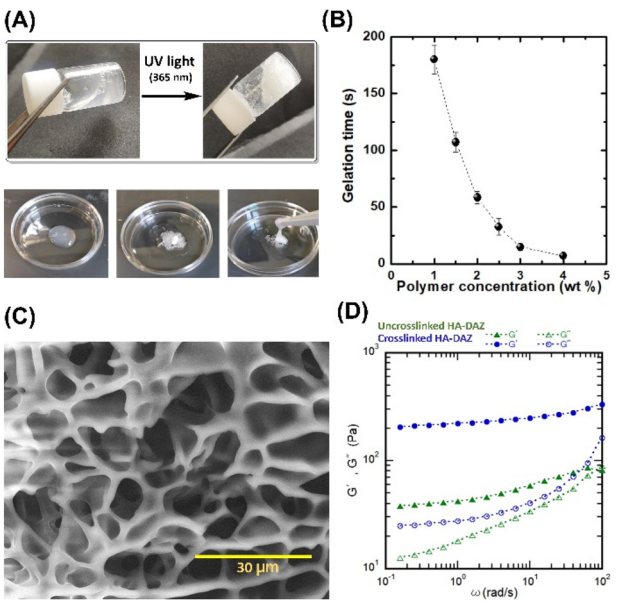

Fig. 3 Gelation of the HA–DAZ/DPI solution due to UV irradiation. (A) Upper panel: UV crosslinked HA–DAZ/DPI hydrogel. Lower panel: Gelation time measurement using the magnetic bar stop method. During the reaction, N_2 bubbles were generated in the hydrogel following UV irradiation. (B) The effect of polymer concentration on gelation time (n = 4). (C) Cross-sectional SEM image of a photocrosslinked HA–DAZ/DPI hydrogel. (D) Frequency sweep of HA–DAZ/DPI before and after photocrosslinking.

3.3 Shear-thinning and self-healing properties of the HA–DAZ/DPI precursor solutions and the photocrosslinked HA–DAZ/DPI hydrogel

Hydrogels designed for injection must show excellent injectability to be useful. Here, the strong shear-thinning behavior of the HA–DAZ/DPI solution was detected using a flow curve before crosslinking at 25 °C (Fig. 4A). Moreover, the viscosity of the HA–DAZ/DPI solution decreased as the shear rate increased. This coincided with rheological measurements (Fig. 3D) in which the HA–DAZ/DPI precursor polymer solution showed similar G' and G'' values. Since the mixture of unmodified HA and DPI showed stronger shear-thinning than that of

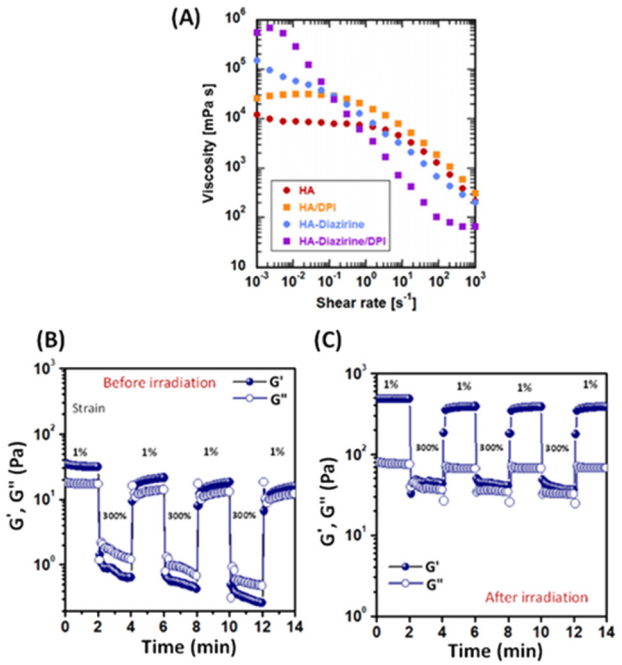

Fig. 4 Shear-thinning and self-healing properties of the HA–DAZ/DPI solution and hydrogel. (A) Flow curves of the HA, HA–DAZ, HA/DPI, and HA–DAZ/DPI solutions. (B and C) Self-healing properties indicated by an alternative strain sweep before (B) and after (C) photocrosslinking.

HA, electrostatic interactions likely contributed to the shear-thinning behavior of the HA–DAZ/DPI precursor polymer solution. Furthermore, hydrophobic interactions also likely contributed to this behavior since the HA–DAZ solution exhibited greater shear-thinning than that exhibited by HA alone. In addition, the fact that the HA–DAZ/DPI solution had the strongest shear-thinning of all the solutions suggested that intermolecular interactions likely functioned to coordinate this effect in the solution. The ratio of the viscosity at 10^{-3} s^{-1} to that at 10^{3} s^{-1} was $>10^{4}$, which is as high as that found in carbomers (carbopols) as well as in commercially available shear-thinning hydrogels composed of crosslinked polyacrylic acid.[40]

Alternative strain sweeps of the HA–DAZ/DPI precursor polymer solution revealed a repeated sol–gel transition induced by shearing (Fig. 4B). The restructuring time from sol to gel was <10 s, which is sufficiently rapid to prevent dripping from the injection site. Moreover, when HA–DAZ was photocrosslinked with DPI *via* covalent bonding, the sol–gel transition was still observed, and the degree of shear-thinning became more pronounced. Taken together these effects suggest that the number of covalent bonds was not as high as the number of physical intermolecular interactions, even after photoirradiation (Fig 4C). Furthermore, these results indicate the usefulness of the developed hydrogel as an injectable self-healing material. The obtained results were not significantly altered when the temperature was changed from 25 °C to 37 °C (Fig. S7†). The effect of the mixing ratio of HA–DAZ and DPI was also examined in Fig. S8A–C.† The volume ratio of HA–DAZ and DPI precursor polymer solution was varied as 1 : 0.5, 1 : 1, and 1 : 1.5, leading to the molar ratio of DAZ/NH_2 as 1 : 8, 1 : 16, and 1 : 24. As a result, it was found that the mechanical property of HA–DAZ/DPI hydrogel increased with decreasing amount of DPI.

3.4 Cytocompatibility of the photocrosslinked HA–DAZ/DPI hydrogel

Next, the cytocompatibility of HA–DAZ and photocrosslinked HA–DAZ/DPI hydrogel was assessed using NIH3T3 fibroblastic cells. This test aimed to determine the toxicity induced by the introduction of the diazirine moiety to HA and the crosslinking with DPI. Although unmodified HA exhibited excellent cytocompatibility at concentrations of ≤0.2% (Fig. 5A), cell viability decreased as the concentration of HA–DAZ increased above 0.2%. In addition, DPI showed a stronger negative effect on cell viability than HA–DAZ due to its cationic nature (Fig. S9A†). In contrast, the photocrosslinked HA–DAZ/DPI hydrogel showed excellent cytocompatibility. Fig. 5B shows the cell viability of NIH3T3 cells incubated with HA–DAZ/DPI hydrogels without direct contact (*i.e.*, using the cell culture insert). We found that cell viability was not affected by increasing the amount of hydrogel and was similar (90–100%) for hydrogel sample weights of 0.1, 0.2, and 0.4 g per well. Moreover, even under direct contact between hydrogels and cells, cell viability was higher than 70% within the examined dose range, suggesting good cytocompatibility (Fig. S9B†). The fact that the HA–DAZ/DPI hydrogels showed higher cytocompatibility than their precursor polymers (*i.e.*, HA–DAZ and DPI) may be due to their fixation inside the hydrogel matrix. By photocrosslinking, precursor polymers become fixed in the

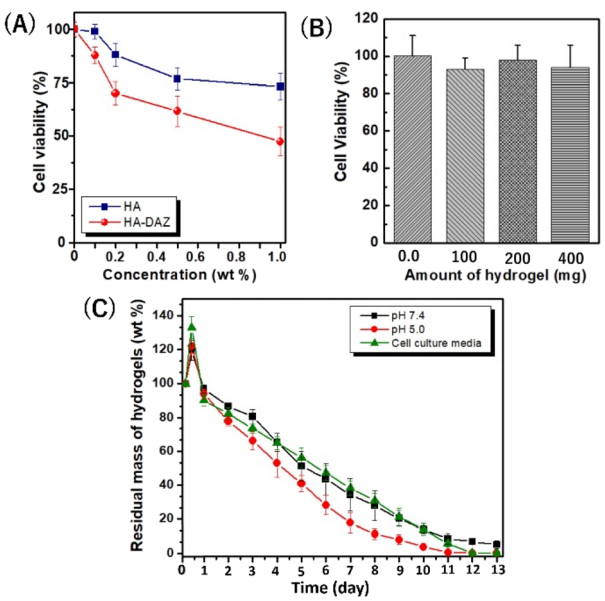

Fig. 5 Cytocompatibility and biodegradability of the HA–DAZ/DPI hydrogel. (A) Cell viability of NIH3T3 cells in the presence of different HA and HA–DAZ concentrations. (B) Cell viability relative to the amount of HA–DAZ hydrogel applied. (C) Swelling and degradation of HA–DAZ/DPI hydrogels at different pH values (n = 4).

hydrogel matrix, which prevents their free diffusion to cells. As a result, although the precursor polymers showed some degree of cytotoxicity, this was strongly reduced after photo-crosslinking. It should be noted that for their *in vivo* application, there is a possibility that free DAZ exposed on the hydrogel surface, as well as that contained in degraded products, may induce toxicity within tissue. Further research is needed to establish the safety of HA–DAZ/DPI hydrogels *in vivo*.

3.5 Swelling and degradation kinetics of the photocrosslinked HA–DAZ/DPI hydrogel

Hydrogel swelling and degradation are important properties for biomedical applications. Although the diazirine moiety is extremely hydrophobic due to its benzene ring and fluorine, HA–DAZ can dissolve in the water due to the high hydrophilicity of HA.

The swelling of the photocrosslinked HA–DAZ/DPI hydrogel was observed at pH 7.4 and 5.0 in PBS (Fig. 5C). The maximum swelling of the hydrogel was attained at 6 h at pH 5.0, pH 7.4, and cell culture medium. After the maximum swelling at pH 5.0, pH 7.4, and cell culture medium, the hydrogels were gradually degraded for approximately 2 weeks. The degradation rate of the hydrogel at pH 5 was slightly higher than that at pH 7.4. Since HA–DAZ has an anionic nature due to the presence of a carboxylic group in HA, and DPI has a cationic nature due to its primary, secondary, and tertiary amines, there is likely an electrostatic interaction between them. This electrostatic interaction can be altered by pH due to changes in the degree of deprotonation/protonation. Therefore, we concluded that this electrostatic interaction may cause differences in the swelling and degradation behaviour of HA–DAZ/DPI hydrogels between pH 5.0 and pH 7.4. Taken together, the favourable degradability values and low toxicity suggest that the photocrosslinked HA–DAZ/DPI hydrogel may be useful for various medical applications in the future.

3.6 Bioadhesion and burst pressure resistance tests of the photocrosslinked HA–DAZ/DPI hydrogel

The bioadhesion of hydrogels can prevent their slippage from the target trauma site *in vivo*: thus, bioadhesion is important for developing new wound dressings, tissue sealants, hemostats, and scaffolds for tissue engineering. Moreover, good bioadhesion can help promote biointegration, biocompatibility, and tissue regeneration under physiological conditions.[41] To evaluate the *ex vivo* bioadhesion efficacy of the photocrosslinked HA–DAZ/DPI hydrogel, lap shear tensile tests were performed (Fig. 6A and B).

During tensile tests, the elongation force increased with extension, and the sample finally fractured at a maximum force. The adhesion strength of photocrosslinked HA–DAZ/DPI and fibrin glue samples were 1600 ± 110 Pa and 1550 ± 87 Pa, respectively (Fig. 6C). In contrast, the adhesion strength of the HA–DAZ/DPI solution was 480 ± 7.4 Pa. Furthermore, application of the only HA–DAZ solution and subsequent photoirradiation also resulted in a comparable adhesion strength (1586 ± 316 Pa) as the photocrosslinked HA–DAZ/DPI hydrogel

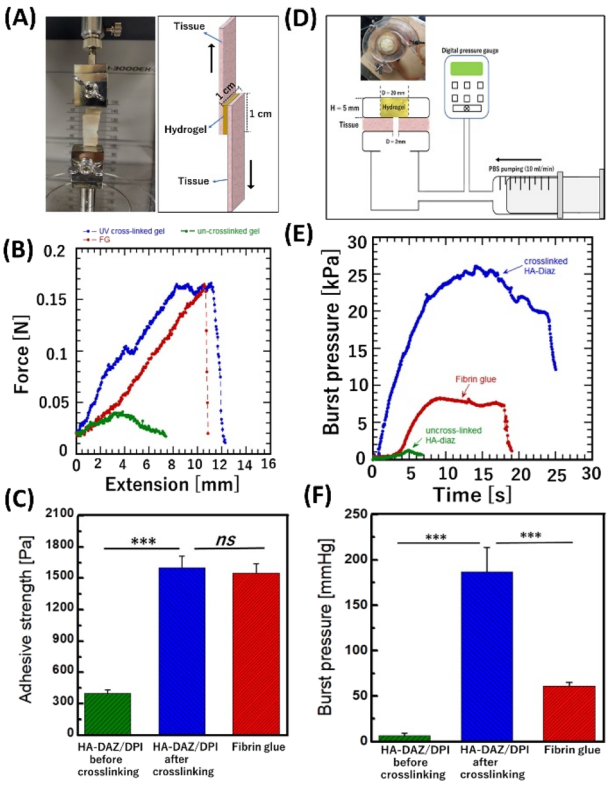

Fig. 6 Bioadhesion and burst pressure resistance of photocrosslinked HA–DAZ/DPI hydrogels. Bioadhesion tests examined adhesion to porcine esophageal mucosa and burst pressure tests tested hydrogel blockage of a pinhole in porcine esophageal mucosa samples. (A) Experimental setup for the lap-shear test. (B) Force curve of the lap shear test. (C) Comparison of the adhesive strength of the photocrosslinked HA–DAZ/DPI hydrogel and fibrin glue. (D) Schematic illustration of the burst pressure test. (E) Pressure time course for the burst test. Pressure increased gradually while the water pressure of the syringe pump was kept at a constant flow rate; hydrogels burst under pressure at the indicated pressure value. (F) Comparison of the burst pressure of photocrosslinked HA–DAZ/DPI hydrogels and fibrin glue. Data are shown as mean ± standard deviation. ANOVA results: $*p < 0.05$, $**p < 0.01$, and $***p < 0.001$.

(Fig. S10†). Taken together, these results suggest that photocrosslinked HA–DAZ/DPI hydrogels show a higher adhesive strength than the fibrin glue and uncrosslinked HA–DAZ/DPI solution since the UV-reactive DAZ moiety reacts with a primary amine of the substrate tissue. In addition, the increase in shear moduli due to crosslinking between DAZ and the amine may have prevented cohesion failure. The time-dependent adhesion strength of HA–DAZ/DPI hydrogels under wet conditions was compared with fibrin glue using porcine esophageal mucosa *via* lap shear testing. Both HA–DAZ/DPI and fibrin glue lost their tissue adhesiveness after 24 hours and 48 hours, respectively (Fig. S11†)

The burst pressure of photocrosslinked HA–DAZ/DPI (Fig. 6D and Fig. S12A†) was significantly higher than that of fibrin glue. Fig. 6E shows that an increase in chamber pressure caused by flow from the syringe pump induced the deformation of set hydrogels. After plastic deformation, the hydro-

gels ruptured, and the maximum pressure recorded was defined as the burst pressure. The burst pressure of the photocrosslinked HA–DAZ/DPI hydrogel was 187 ± 27 mmHg (24.9 ± 3.6 kPa), which is approximately three times higher than that of fibrin glue (61 ± 4 mmHg; 8.1 ± 0.5 kPa) (Fig. 6F). Moreover, the burst pressure of the uncrosslinked HA–DAZ/DPI solution was 7.6 ± 2.6 mmHg (1.0 ± 0.3 kPa), which is much lower than that of fibrin glue. It has been reported that PAMAM-*g*-diazirine displayed a burst pressure of 60 to 345 mmHg (8 to 46 kPa) against collagen/cellulose films. These films are soft tissue-mimicking films based on collagen cellulose composite films used for *in vitro* assessment of various biomedical and diagnostics applications and showed a burst pressure of 47.4 ± 10.4 mmHg (6.3 ± 1.38 kPa) against the porcine esophagus. In contrast, a mixture of chitosan, 1-(3-dimethylaminopropyl)-3-ethylcarbodiimide hydrochloride (EDC), and *N*-hydroxy succinimide showed a burst pressure of 160 mmHg (21.33 kPa) against porcine hepatic portal vein tissue. Although it is difficult to compare these values directly since burst pressures are measured against different tissues using different methods, the burst pressure of the photocrosslinked HA–DAZ/DPI hydrogel was within a similar range. It was also higher than the systolic blood pressure found in healthy individuals (*i.e.*, 120 mmHg or 15.99 kPa) as well as intestine pressure (*i.e.*, 3 to 30 kPa). Therefore, these results indicate that the photocrosslinked HA–DAZ/DPI hydrogel is a promising material for use as a sealing hemostat. After the rupture of the hydrogels in a burst pressure test, we observed adhesion failure at the applied positions of the HA–DAZ/DPI hydrogel and fibrin glue over the substrate tissue. In this case, the hydrogels were not punctured but were separated from the substrate tissue. However, uncrosslinked HA–DAZ could not form a rigid gel; therefore, cohesion failure was observed before adhesion failure.

4. Discussion

Diazirine is a photoreactive moiety that allows *in situ* crosslinking *via* the formation of carbene, which is highly reactive with primary amines and produces no toxic byproducts. Diazirine and its conjugates are also stable in both acidic and basic environments as well as under ambient light exposure during routine chemical synthesis,[42,43] Here, we report the first test of diazirine-conjugated HA and an associated photocrosslinking injectable hydrogel. Moreover, to the best of our knowledge, this study is the first in which diazirine was conjugated with any natural polysaccharide. Despite the hydrophobic diazine moiety of HA–DAZ, due to its extremely hydrophilicity of the HA backbone, the obtained HA–DAZ material was water soluble. Several photoreactive functional groups, including aryl azide and benzophenone, are often used during the development of photocrosslinkable materials. However, diazirine has several advantages over these groups, including its activation at a wavelength of light (~355 nm) that does not induce severe damage to nearby proteins.

The injectability of hydrogels is critically important for biomedical applications. Some researchers are designing shear-thinning hydrogels that exhibit smooth flowability under shear stress, *i.e.*, shear-thinning, and can recover when the applied stress is removed. This prevents spillage of the material from the applied site in response to high-yield stress.[44] Interestingly, the shear-thinning behavior of HA–DAZ and HA–DAZ/DPI were comparatively higher than that of unmodified HA (Fig. 4). This shear-thinning behavior likely originated from hydrophobic interactions between diazirine moieties and the ionic interaction between the carboxylic groups of HA and the amine groups of DPI (Fig. 7). Due to their hyperbranched structure and multiple amine groups, DPIs function as physical crosslinkers with multiple electrostatic interactions.[45] Here, multiple amine groups likely contributed to the efficient chemical crosslinking between the diazirine moieties of HA–DAZ after photocuring, thereby altering the bulk structure of the hydrogel and strengthening its shear-thinning properties. However, the mechanical strength of the hydrogel decreases when an excess molar amount of DPI is incorporated, and *vice versa*, probably because the excess DPI reduces the probability of crosslinking between two HA–DAZ chains. Therefore, the mechanical strength of the hydrogel matrix would have decreased from the 1.5% to 0.5% HA–DAZ/DPI ratio (Fig. S8†). In addition, the synthesized HA–DAZ in this research had acyl urea modification by the side reaction. Moreover, researchers have reported that the photocrosslinking reaction can be affected by the presence of acyl urea through quenching the radicals *via* intramolecular reactions.[46] To minimize intramolecular rearrangement reactions with EDC, HOBt is usually added before the addition of EDC.[47,48] Further optimization of the conjugation reaction condition would increase the mechanical strength of HA–DAZ after photocuring.

The shear-thinning behavior enables the injection of the hydrogel through needles and catheters and thereby makes HA–DAZ suitable for tissue adhesion applications. In addition, this behavior may also be useful for 3D bioprinting technology when using dispensers for scaffolding fabrication in tissue engineering. HA-based photocrosslinking bio-inks for 3D printing could aid the development of tissue scaffolds due to their excellent biocompatibility.[49,50]

Photocured and polymeric tissue adhesives are attracting increased interest for use in surgery because they can replace

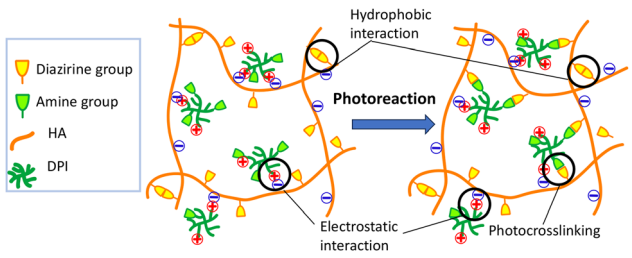

Fig. 7 Schematic illustration of the hypothesized bulk structure of the HA–DAZ/DPI solution and the photocrosslinked hydrogel.

conventional sutures and have several advantageous properties, including anti-infection and hemostatic properties, and the possibility of rapid wound closure.[51] The clinical application of these tissue adhesives requires that they be biocompatible, nonimmunogenic, and do not cause inflammation or other toxicity issues.[52] Fibrin glues are widely used in clinical settings and are known to have good biocompatibility, but they are not strongly adhesive, and the risk of infection transmission limits their applicability. Thus, a new type of bioadhesive is required that possesses tuneable adhesive strength, but is also fast curing, shows excellent biocompatibility, and shows high biodegradability. Diazirine-based synthetic polymer hydrogels have been reported previously by Steele *et al.*, who developed a diazirine-grafted PLGA film for bioadhesion applications.[24,30] In such a design, the diazirine moiety can form a covalent bond between a thin film or hydrogel and a tissue amine group, thereby increasing adhesiveness. PAMAM-*g*-diazirine-based[30] formulations were found to have tuneable shear moduli of 1–100 kPa and maximum shear adhesion strength of 27 kPa when attached to wet *ex vivo* arteries; this was higher than the adhesion strength of fibrin glue.[24,53] Diazirine[54]-based polymers are as promising as aryl azide-based polymers[44] in this respect. Table S1† compares the UV light intensity, exposure time, and adhesion strength of previously reported diazine-based hydrogels with those of HA–DAZ/DPI hydrogels. This comparison suggests that HA–DAZ/DPI hydrogels can be formed *via* photoirradiation with relatively low power (6 mW cm^{-2}) using a short exposure time (*i.e.*, five minutes). HA shows excellent biocompatibility and frequently contributes to the maintenance of a moist environment for effective wound healing.[55] For example, Martínez-Sanz *et al.*[56] reported aldehyde and hydrazide-modified HA-based hydrogels that were used as a BMP-2 carrier to promote bone augmentation. Furthermore, Jin *et al.*[57] developed a tyramine-conjugated HA as an injectable anti-inflammatory hyaluronic acid hydrogel for osteoarthritic cartilage repair. Here, HA–DAZ exhibited excellent cytocompatibility (Fig. 5) and excellent adhesiveness (Fig. 6). Thus, HA–DAZ/DPI has potential as biocompatible tissue adhesives.

In fact, recent advances in diazirine-based tissue adhesives have been remarkable: *In vitro* bacterial reverse mutation assay (Ames OECD 471) and skin sensitization analysis have demonstrated for the first time the excellent safety profile of diazirine-grafted polycaprolactone tetrol.[58] In addition, various liquid additives containing reactive functional groups such as hydroxyl, thiol, amine, or acrylate are being combined with diazirine derivatives, and the chemical structure design of diazirine-based tissue adhesives is becoming increasingly diverse.[59] Iridium photocatalysts have also been reported to allow photoreaction of diazirine with blue visible light at 445 nm,[60] avoiding the use of UV-A, as well as the possibility of using diazirine as an adhesive that does not react in room light but does react in sunlight.[61] Finally, the use of diazirine-based photocurable tissue adhesives for the fixation of transparent bone pins was reported as a potential medical application.[62] Considering that recent studies have demonstrated the safety and biocompatibility of diazirine-based light-cured tissue adhesives, which have long been pointed out,[63] the HA–DAZ reported in this study is a diazirine conjugate with HA, which is widely used in the body. Further studies as an adhesive are expected.

5. Conclusions

In this paper, we report the first design and synthesis of an injectable photocrosslinking HA–DAZ and DPI system. The HA-DAZ solution described here formed a physical hydrogel, likely due to electrostatic and hydrophobic interactions, and exhibited shear-thinning and self-healing properties as well as good cytocompatibility. It was also photocurable *via* photocrosslinking between a UV-activated diazirine moiety and the primary amine group. After photocuring, the HA-DAZ hydrogels exhibited improved self-healing, shear-thinning, and cytocompatibility relative to the HA–DAZ solution. In addition, the HA–DAZ/DPI hydrogel exhibited excellent bioadhesiveness due to a reaction between the primary amine groups of tissue proteins and the diazirine of HA–DAZ. Consequently, the HA–DAZ/DPI hydrogel also showed a higher burst pressure than fibrin glue. In summary, the novel photocrosslinkable, injectable, and shear-thinning HA–DAZ/DPI hydrogel reported here is a promising candidate for tissue sealant applications.

Author contributions

Arvind K. Singh Chandel: investigation, visualization, writing original draft preparation, Athira M. Sreedevi: investigation, Saki Okada, Zhang Qiming: investigation, Natsuko F. Inagaki: investigation, Seiichi Ohta: investigation, supervision, writing – review & editing, Taichi Ito: conceptualization (total), writing – review & editing, funding acquisition, project administration, supervision.

Conflicts of interest

The authors have no conflicts of interest to declare.

Acknowledgements

This work was supported by two grants from JSPS KAKENHI (no. 17K19006 and 19F19061).

References

1 J. Necas, L. Bartosikova, P. Brauner and J. Kolar, *Vet. Med.*, 2008, **53**, 397–411.
2 L. Lapcık Jr., L. Lapcık, S. De Smedt, J. Demeester and P. Chabrecek, *Chem. Rev.*, 1998, **98**, 2663–2684.

3 C. B. Highley, G. D. Prestwich and J. A. Burdick, Recent advances in hyaluronic acid hydrogels for biomedical applications, *Curr. Opin. Biotechnol.*, 2016, **40**, 35–40.
4 J. A. Burdick and G. D. Prestwich, *Adv. Mater.*, 2011, **23**, H41–H56.
5 Y. Yeo, C. B. Highley, E. Bellas, T. Ito, R. Marini, R. Langer and D. S. Kohane, *Biomaterials*, 2006, **27**, 4698–4705.
6 X. Z. Shu, Y. Liu, Y. Luo, M. C. Roberts and G. D. Prestwich, *Biomacromolecules*, 2002, **3**, 1304–1311.
7 R. Jin, L. M. Teixeira, A. Krouwels, P. J. Dijkstra, C. A. Van Blitterswijk, M. Karperien and J. Feijen, *Acta Biomater.*, 2010, **6**, 1968–1977.
8 A. Takahashi, Y. Suzuki, T. Suhara, K. Omichi, A. Shimizu, K. Hasegawa, N. Kokudo, S. Ohta and T. Ito, *Biomacromolecules*, 2013, **14**, 3581–3588.
9 S. D. Kim, S. Jin, S. Kim, D. Son and M. Shin, *Polymers*, 2022, **15**, 3173.
10 Y. Li, Z. Li, Y. Bao, T. Chen, Y. Cheng and M. Xu, *Front. Bioeng. Biotechnol.*, 2021, **9**, 1272.
11 Y. W. Ding, Z. Y. Wang, Z. W. Ren, X. W. Zhang and D. X. Wei, *Biomater. Sci.*, 2022, **10**, 3393–3409.
12 H. Suo, M. Hussain, H. Wang, N. Zhou, J. Tao, H. Jiang and J. Zhu, *Biomacromolecules*, 2021, **22**, 3049–3059.
13 J. Yeom, S. H. Bhang, B. S. Kim, M. S. Seo, E. J. Hwang, I. H. Cho, J. K. Park and S. K. Hahn, *Bioconjugate Chem.*, 2010, **21**, 240–247.
14 E. J. Strauss, J. A. Hart, M. D. Miller, R. D. Altman and J. E. Rosen, *Am. J. Sports Med.*, 2009, **37**, 1636–1644.
15 L. K. Widjaja, M. Bora, P. N. P. H. Chan, V. Lipik, T. T. Wong and S. S. Venkatraman, *J. Biomed. Mater. Res., Part A*, 2014, **102**, 3056–3065.
16 L. Ouyang, C. B. Highley, C. B. Rodell, W. Sun and J. A. Burdick, *ACS Biomater. Sci. Eng.*, 2016, **2**, 1743–1751.
17 Q. Yang, J. Peng, H. Xiao, X. Xu and Z. Qian, *Carbohydr. Polym.*, 2022, **278**, 118952.
18 J. Baier Leach, K. A. Bivens, C. W. Patrick Jr. and C. E. Schmidt, *Biotechnol. Bioeng.*, 2003, **82**, 578–589.
19 X. Jia, J. A. Burdick, J. Kobler, R. J. Clifton, J. J. Rosowski, S. M. Zeitels and R. Langer, *Macromolecules*, 2004, **37**, 3239–3248.
20 K. W. Chun, J. B. Lee, S. H. Kim and T. G. Park, *Biomaterials*, 2005, **26**, 2819–3326.
21 R. A. Alatawi, M. Monier and N. H. Elsayed, *Process Biochem.*, 2020, **88**, 67–77.
22 R. F. Pereira, C. C. Barrias, P. J. Bártolo and P. L. Granja, *Acta Biomater.*, 2018, **66**, 282–293.
23 J. Zhang, Y. Yang, Y. Chen, X. Liu, S. Guo, L. Zhu and Y. Wang, *J. Mater. Chem. B*, 2016, **4**, 973–981.
24 V. Mogal, V. Papper, A. Chaurasia, G. Feng, R. Marks and T. W. J. Steele, *Macromol. Biosci.*, 2014, **14**, 478–484.
25 R. Beninatto, C. Barbera, O. De Lucchi, G. Borsato, E. Serena, C. Guarise, M. Pavan, C. Luni, S. Martewicz, D. Galesso and N. Elvassore, *Mater. Sci. Eng., C*, 2019, **96**, 625–634.
26 H. J. Lee, G. M. Fernandes-Cunha and D. Myung, *Funct. Polym.*, 2018, **131**, 29–35.
27 G. Wang, X. Cao, H. Dong, L. Zeng, C. Yu and X. Chen, *Polymers*, 2018, **10**, 949.
28 M. W. Halloran and J. P. Lumb, *Chem. – Eur. J.*, 2019, **25**, 4885–4898.
29 A. L. MacKinnon and J. Taunton, *Curr. Protoc. Chem. Biol.*, 2009, **1**, 55–73.
30 F. Gao, I. Djordjevic, O. Pokholenko, H. Zhang, J. Zhang and T. W. J. Steele, *Molecules*, 2018, **23**, 796.
31 Y. Wang, X. Wang and J. K. Montclare, *Biomacromolecules*, 2021, **22**, 1509–1522.
32 Y. Wang, E. Delgado-Fukushima, R. X. Fu, G. S. Doerk and J. K. Monclare, *Biomacromolecules*, 2020, **21**, 3608–3619.
33 C. Loebel, C. B. Rodell, M. H. Chen and J. A. Burdick, *Nat. Protoc.*, 2017, **12**, 1521–1541.
34 A. S. Madhavikutty, S. Ohta, A. K. S. Chandel, P. Qi and T. Ito, *J. Chem. Eng. Jpn.*, 2021, **54**, 500–511.
35 C. B. Rodell, M. E. Lee, H. Wang, S. Takebayashi, T. Takayama, T. Kawamura, J. S. Arkles, N. N. Dusaj, S. M. Dorsey, W. R. Witschey and J. J. Pilla, *Circ.: Cardiovasc. Interventions*, 2016, **9**, e004058.
36 B. von Lospichl, S. Hemmati-Sadeghi, P. Dey, T. Dehne, R. Haag, M. Sittinger, J. Ringe and M. Gradzielski, *Colloids Surf., B*, 2017, **159**, 477–483.
37 L. Ouyang, J. P. Armstrong, Y. Lin, J. P. Wojciechowski, C. Lee-Reeves, D. Hachim, K. Zhou, J. A. Burdick and M. M. Stevens, *Sci. Adv.*, 2020, **6**, eabc5529.
38 M. Okawa, M. Sakoda, S. Ohta, K. Hasegawa, Y. Yatomi and T. Ito, *Biomacromolecules*, 2020, **21**, 2695–2704.
39 Y. Hong, F. Zhou, Y. Hua, X. Zhang, C. Ni, D. Pan, Y. Zhang, D. Jiang, L. Yang, Q. Lin and Y. A. Zou, *Nat. Commun.*, 2019, **10**, 1–11.
40 A. O. Andrade, M. E. Parente and G. Ares, *Braz. J. Pharm. Sci.*, 2014, **50**, 931–941.
41 H. Li, R. Niu, J. Yang, J. Nie and D. Yang, *Carbohydr. Polym.*, 2011, **86**, 1578–1585.
42 D. M. Dankbar and G. A. Gauglitz, *Anal. Bioanal. Chem.*, 2006, **386**, 1967–1974.
43 S. S. Ge, B. Chen, Y. Y. Wu, Q. S. Long, Y. L. Zhao, P. Y. Wang and S. Yang, *RSC Adv.*, 2018, **8**, 29428–29454.
44 T. Wang, J. Nie and D. Yang, *Carbohydr. Polym.*, 2012, **90**, 1428–1436.
45 D. Appelhans, H. Komber, M. A. Quadir, S. Richter, S. Schwarz, J. van der Vlist, A. Aigner, M. Müller, K. Loos, J. Seidel and K. F. Arndt, *Biomacromolecules*, 2009, **10**, 1114–1124.
46 S. Samanta, V. K. Rangasami, N. A. Murugan, V. S. Parihar, O. P. Varghese and O. P. Oommen, *Polym. Chem.*, 2021, **20**, 2987–2991.
47 T. Wan, P. Fan, M. Zhang, K. Shi, X. Chen, H. Yang and Y. Zhou, *ACS Appl. Bio Mater.*, 2021, **1**, 334–343.
48 S. Samanta, L. Ylä-Outinen, V. K. Rangasami, S. Narkilahti and O. P. Oommen, *Acta Biomater.*, 2022, **140**, 314–323.
49 C. E. Schanté, G. Zuber, C. Herlin and T. F. Vandamme, *Carbohydr. Polym.*, 2011, **85**, 469–489.

50 C. Yu, H. Gao, Q. Li and X. Cao, *Polym. Chem.*, 2020, **11**, 3169–3178.
51 M. Ishihara, K. Obara, S. Nakamura, M. Fujita, K. Masuoka, Y. Kanatani, B. Takase, H. Hattori, Y. Morimoto, M. Ishihara and T. Maehara, *J. Artif. Organs*, 2006, **9**, 8–16.
52 L. Zhou, C. Dai, L. Fan, Y. Jiang, C. Liu, Z. Zhou, P. Guan, Y. Tian, J. Xing, X. Li and Y. Luo, *Adv. Funct. Mater.*, 2021, **31**, 2007457.
53 Y. Liu, X. Yang, X. W. Shi, W. E. Bentley and G. F. Payne, *ACS Symp. Ser.*, 2010, 35–44.
54 M. K. McDermott, T. Chen, C. M. Williams, K. M. Markley and G. F. Payne, *Biomacromolecules*, 2004, **5**, 1270–1279.
55 Y. W Ding, Z. Y. Wang, Z. W. Ren, X. W Zhang, and D. X. Wei, *Biomater. Sci.*, 2022, **10**, 3393–3409.
56 E. Martínez-Sanz, D. A. Ossipov, J. Hilborn, S. Larsson, K. B. Jonsson and O. P. Varghese, *J. Controlled Release*, 2011, **152**, 232–240.
57 Y. Jin, R. H. Koh, S. H. Kim, K. M. Kim, G. K. Park and N. S. Hwang, *Mater. Sci. Eng., C*, 2020, **115**, 111096.
58 I. Djordjevic, G. Wicaksono, I. Solic and T. W. J. Steele, *Macromol. Rapid Commun.*, 2020, **41**, 2000235.
59 E. Ellis, I. Djordjevic, M. N. Bin Mohd Ali and T. W. J. Steele, *ACS Appl. Polym. Mater.*, 2023, **5**, 1440–1452.
60 I. Djordjevic, G. Wicaksono, I. Solic, J. Singh, T. S. Kaku, S. Lim, E. Wei, J. Ang, L. Blancafort and T. W. J. Steele, *ACS Appl. Mater. Interfaces*, 2021, **13**, 36839–36848.
61 N. C. S. Tan, I. Djordjevic, J. A. Malley, A. L. Q. Kwang, S. Ikhwan, I. Solic, J. Singh, G. Wicaksono, S. Lim and T. W. J. Steele, *Mater. Sci. Eng., C*, 2021, **127**, 112240.
62 G. Wicaksono, F. Toni, L. Wei Feng Tok, J. J. T. Thng, I. Solic, M. Singh, I. Djordjevic, F. Baino and T. W. J. Steele, *ACS Biomater. Sci. Eng.*, 2021, **7**, 4463–4473.
63 R. D. O'Rorke, O. Pokholenko, F. Gao, T. Cheng, A. Shah, V. Mogal and T. W. J. Steele, *Biomacromolecules*, 2017, **18**, 674–682.